

CLIP Brings Better Features to Visual Aesthetics Learners

Liwu Xu[†], Jinjin Xu[†], Yuzhe Yang, Yijie Huang, Yanchun Xie, Yaqian Li^{*}
OPPO Research Institute

{xuliwu, jinxu95, yangyuzhe, huangyijie, xieyanchun, liyaqian}@oppo.com

Abstract

The success of pre-training approaches on a variety of downstream tasks has revitalized the field of computer vision. Image aesthetics assessment (IAA) is one of the ideal application scenarios for such methods due to subjective and expensive labeling procedure. In this work, an unified and flexible two-phase CLIP-based Semi-supervised Knowledge Distillation paradigm is proposed, namely CSKD. Specifically, we first integrate and leverage a multi-source unlabeled dataset to align rich features between a given visual encoder and an off-the-shelf CLIP image encoder via feature alignment loss. Notably, the given visual encoder is not limited by size or structure and, once well-trained, it can seamlessly serve as a better visual aesthetic learner for both student and teacher. In the second phase, the unlabeled data is also utilized in semi-supervised IAA learning to further boost student model performance when applied in latency-sensitive production scenarios. By analyzing the attention distance and entropy before and after feature alignment, we notice an alleviation of feature collapse issue, which in turn showcase the necessity of feature alignment instead of training directly based on CLIP image encoder. Extensive experiments indicate the superiority of CSKD, which achieves state-of-the-art performance on multiple widely used IAA benchmarks.

1. Introduction

The advent and success of unsupervised and multi-modal pre-training, such as GPTs [1, 21, 22] and CLIP [20], have brought deep learning into a whole new era. Nevertheless, in the field of computer vision, the benefits of scaling up the model and data volumes are not as great as in natural language processing tasks, which may be caused by the low information density of visual inputs. Hence, leveraging cross-modal information becomes more and more popular for visual pre-training.

Image aesthetics assessment (IAA), as a traditional computer vision task, aims at evaluating the aesthetic perception of an image automatically and has been broadly applied in various areas, such as image enhancement [26], personalized photo album management [36] and etc. However, IAA task suffers from the poor model generalization ability due to the complex, non-uniform and expansive annotating process [28]. In the early stage, researchers dedicate themselves to developing hand-crafted features [13], while the representation ability of such features is not sufficient to capture complicated human perception. Fortunately, the emerging DL-based IAA algorithms show great potential in solving this problem [12, 27]. For example, Talebi et al. propose a simple-yet-effective scheme called NIMA that far exceeds the performance of hand-crafted methods [27]. Recently, various deep learning (DL) based methods have been proven to be effective, such as multi-patch aggregation [35], composition-aware IAA [24] and multi-scale feature fusion [12]. Furthermore, the transfer of knowledge between semantic features and aesthetics features has garnered significant attention among researchers, resulting in state-of-the-art outcomes [8, 11].

The high time & space complexity of most DL-based methods make them hard to be deployed on mobile devices, and the lightweight design of such methods usually leads to an unacceptable performance drop. This is because the reduced image size and degenerated model capability amplify the error of the algorithms. One natural proposal is to enhance the performance of the on-device model by knowledge distillation, but a curious phenomenon undermines this hypothesis: without massive data volume, the lightweight student IAA model shows minor improvements even with a large, well-trained teacher model in a supervised manner.

In response to this, a novel CLIP-based two-phase Semi-supervised Knowledge Distillation method is proposed in this work, namely CSKD, which not only improves the generalization ability but also enhances the knowledge distillation efficiency of IAA algorithms. As illustrated in Fig. 1, we firstly utilize a large amount of unlabeled data (3 million) to align the features of the visual encoders and CLIP image encoder/backbone with no constraints on the model structure.

^{*}Corresponding author.

[†]Equal contribution.

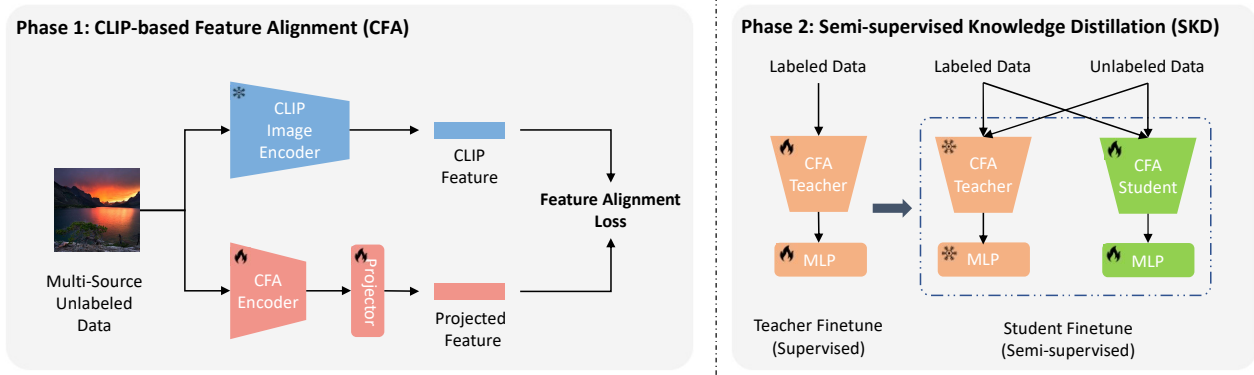


Figure 1. The overall workflows of CSKD (including CFA and SKD). CFA starts with ImageNet pre-trained backbones, then distilled unsupervisedly from CLIP with a mixed source unlabeled dataset. In terms of SKD, we first supervisedly fine-tune a teacher based on CFA backbone, then train a CFA-based student in a semi-supervised manner.

Then, the well-trained encoder (e.g., Swin-Base) is combined with a task-specific MLP head and fine-tuned in a supervised manner, which leads to a strong teacher for pseudo label generation. Finally, we train an efficient and generalizable student (e.g., MobileNetV2) via semi-supervised knowledge distillation. Contributions can be summarized in three folds:

- An unified and generalizable unsupervised CLIP-based Feature Alignment (CFA) method is proposed in this paper, and proved to be a good solution for visual encoder pre-training.
- A Semi-supervised Knowledge Distillation (SKD) protocol is presented and proven to be a versatile and effective tool for IAA tasks. Both teacher and student distilled from CLIP show better performance when learning from large-scale unlabeled data.
- The proposed pipeline is evaluated with extensive experiments on commonly used IAA benchmarks. With our protocol, the aforementioned NIMA algorithm can surpass state-of-the-art results.

2. Related Work

2.1. Pre-training

Unsupervised, weak-supervised and self-supervised pre-training techniques have gained a lot of attention in the field of computer vision recently [6]. Among the many efforts, CLIP [20] represents a crucial milestone due to its pioneering use of large-scale web-crawled data for image-text contrastive learning, yielding better feature representation ability and impressive zero-shot performance. And hence, the pre-trained CLIP visual encoder has been widely adopted as the feature extractor for various downstream tasks, such as MaskCLIP [39] and Stable Diffusion [23].

Although the application progress of CLIP in the field of aesthetics has been slow, there have been some insightful works. For example, Wang et al. design a series of general prompts like $\{good/bad\ photos\}$ to assist the assessment of the images [29]. In this paper, we further leverage the representation ability of CLIP to improve the performance of IAA models via knowledge distillation.

2.2. Knowledge & Feature Distillation

Knowledge distillation (KD) [9] is an unified paradigm that enhances the performance of student models through the utilization of both ground truth labels and pseudo labels (hard or soft) generated by proficient teacher(s). KD offers a range of comprehensive benefits, including the reduction of model size and the improvement of model generalization [31]. Nevertheless, we see limited improvements in the student model when normal KD is performed using labeled data only in IAA tasks (refer to Table 6), yet Chen et al. claim that conducting knowledge distillation with unlabeled data can further improve learning efficiency [4], which inspires us to develop a semi-supervised knowledge distillation manner to increase the efficiency of KD.

Feature distillation (FD) is a subclass of KD, where knowledge is transferred by learning feature representations instead of outputs [30]. One crucial distinction between FD and KD lies on the flexibility, where the teacher and student models can originate from different domains, possess varying output dimensions, and exhibit other dissimilarities. Recent works showcase that learnt representations (e.g. CLIP) can be distilled to a untrained model via feature distillation [7, 33]. Inspired by this, we also adopted an off-the-shelf CLIP image encoder as teacher to transfer rich knowledge to our given visual encoder as initialized parameter (followed by a MLP projector).

Notably, there are two major differences in our scheme. 1) Distillation target. We choose to use the CLS token, so

that there is no model structure dependency and spatial alignment issues. 2) Initialization of distilled model. We start with ImageNet pretrained parameters instead of train from scratch for faster convergence and better performance.

3. CSKD: CLIP-based Semi-supervised Knowledge Distillation

As shown in Fig.1, the proposed workflow consists of two phases, CLIP-based feature alignment (CFA) and semi-supervised knowledge distillation (SKD). In terms of phase I, a multi-source (e.g., ImageNet & OpenImages detection subset) unlabeled dataset is introduced to train well generalized backbones (for teacher and student, respectively) for the next stage. In phase II, a teacher model (CFA teacher backbone and a MLP head) is fine-tuned using labeled task-specific data, then both labeled and unlabeled data are used to train the student model (CFA student backbone and a MLP head) in a semi-supervised manner. In the following content, we will introduce components of CSKD separately.

3.1. Phase I: CLIP-based Feature Alignment (CFA)

In this section, we use the off-the-shell CLIP image encoder to adjust the feature distribution of task-specific backbones because, as was already mentioned, the feature collapse problem of CLIP has been alleviated by the plenty of training picture-text pairings. In this way, only unlabeled data is needed because closer feature representations rather than similar logit outputs are what are crucial. The pipeline of CFA phase is illustrated on the left side of Fig. 1.

Specifically, we first create a multi-source unlabeled dataset of around 3M images from ImageNet [5] (1.2M) and OpenImages [15] detection subset (1.9M). Then, given a pre-trained backbone (for example, Swin-Base-In21k from timm [34]), we can further align the representation maps between CLIP image encoder and the given backbone (followed by a MLP projector) via a cosine similarity based alignment loss,

$$\mathcal{L}_{align}(\mathbf{x}_1, \mathbf{x}_2) = 1 - \frac{\mathbf{x}_1 \cdot \mathbf{x}_2}{\max(\|\mathbf{x}_1\|_2 \cdot \|\mathbf{x}_2\|_2, \epsilon)}, \quad (1)$$

where \mathbf{x}_1 and \mathbf{x}_2 are the CLS token of CLIP and the projected feature of the given backbone, respectively. And ϵ is a constant that is usually set to $1e-8$ to avoid zero dividing.

Notably, we train three backbones (e.g., Swin-Base & MV2) in this way for the following phase, referred to as CFA teacher and CFA student, respectively. Discussions about the feature representations before and after alignment are given in Section 6.1.

3.2. Phase II: Semi-supervised Knowledge Distillation

It is typically to fine-tune models with task-specific labeled datasets for downstream tasks. We initially fine-tune

the teacher (formed by a CFA teacher backbone and a MLP head) using AVA [19], AADB [14] or PARA [37] benchmarks. Then, the well-trained teacher is used to supervise the student (formed by a CFA student backbone and a MLP head). The pipeline of phase II can be found on the right hand of Fig. 1. However, in supervised KD settings, a larger teacher does not necessarily produce a better student when there is no enough data. Inspired by a recent study [4], we innovatively optimize the student model on both labeled and unlabeled data by minimizing the squared earth-mover-distance (EMD) [27] between predictions and human-annotated labels or pseudo labels (called semi-supervised knowledge distillation, SKD), which is:

$$\mathcal{L}_{EMD}(\mathbf{p}, \mathbf{q}) = \left(\frac{1}{d} \sum_{i=1}^d |(CDF_{\mathbf{p}}(i) - CDF_{\mathbf{q}}(i))|^r\right)^{1/r}, \quad (2)$$

in which r is a hyper-parameter that is set to 2, $\mathbf{p} \in R^d$ and $\mathbf{q} \in R^d$ represent prediction and target vectors, and CDF refers to the cumulative distribution function, respectively. The objective function of the student model in the SKD stage is:

$$\mathcal{L}_{stu} = \mathcal{L}_s + \beta * \mathcal{L}_{kd}, \quad (3)$$

where β is a fixed balancing factor, and \mathcal{L}_s refers to the loss of supervision:

$$\mathcal{L}_s = \frac{1}{B_s} \sum_{j=1}^{B_s} \mathcal{L}_{EMD}(\mathbf{p}^j, \mathbf{q}^j), \quad (4)$$

where B_s is the size of labeled data per batch, and \mathcal{L}_{kd} is the pseudo label based knowledge distillation loss:

$$\mathcal{L}_{kd} = \frac{1}{B_s + \mu B_s} \sum_{k=1}^{B_s + \mu B_s} \mathcal{L}_{EMD}(\mathbf{p}^u, \hat{\mathbf{q}}^u), \quad (5)$$

in which μ indicates the proportion of unlabeled data, and $\hat{\mathbf{q}}^u$ is the pseudo target vector. Thus, the total batch size B equals to $B_s + \mu * B_s$.

4. Experiments

4.1. Datasets and Evaluation Protocol

Following previous work, three trustworthy benchmark IAA datasets, namely AVA [19], AADB [14] and PARA [37], are adopted to evaluate the performance of the proposed scheme. The number of samples labeled with mean opinion score (MOS) are 242,538, 10,000 and 31,220 of AVA, AADB and PARA, respectively, where 237,623, 8345 and 28220 samples are randomly selected for training.

4.2. Implementation Details

All experiments are conducted with 4 NVIDIA Tesla V100 GPUs and PyTorch framework. Pre-processing starts with scaling the images to a size of 256×256 . Subsequently, a random crop of size 224×224 is applied, and finally, a random horizontal flip is performed with a probability of 0.5. The initial learning rate for all backbones is fixed to 1×10^{-4} , and will decay by a factor of 0.1 at epoch 5 for MV2 and ViT-Tiny, at epoch 2 for Swin-Base, 16 epochs in total. Adam is selected as the optimizer, and μ and β in the SKD stage are both set to 15. Note that before CFA phase, backbones are initialized with ImageNet pre-trained weights (MV2 and ViT-Tiny) or ImageNet-21k (Swin-Base) from timm [34]. Finally, the default image encoder used of CLIP is ViT-L-14.

4.3. Evaluation Metrics

Following previous work, mean squared error (MSE), Spearman rank order cross-correlation coefficient (SRCC) and Pearson linear cross-correlation coefficient (PLCC) are used as the performance indicators. In general, MSE reflects the numeric distance between prediction and ground truth. PLCC and SRCC help to mirror the linear and ranking consistency between model estimation and human annotation. Both PLCC and SRCC range from -1 to 1 and higher value indicates better results.

5. Experimental Results

5.1. Main Results on AVA Dataset

The proposed method is compared with several SOTA methods and the main results are summarized in Table 1. Notably, we include the size of the input image in the table for a fair comparison. It can be observed that the proposed methods CFA and SKD improve the performance with both large (e.g., Swin-Base) and lightweight student (e.g., MV2). We use three different groups of teacher student pairs, Swin-Base \rightarrow MV2, Swin-Base \rightarrow ViT-Tiny and Swin-Base \rightarrow Swin-Base for semi-supervised KD. For supervised settings, NIMA* can be competitive with previous SOTA method [11]. Moreover, there is a big improvement on SRCC and PLCC under the same model structure with CFA backbones, where the only difference is the pre-trained weights: in CFA, backbones are initialized with ImageNet pre-trained weights and then distilled based on CLIP, while in NIMA* backbones are initialized with ImageNet pre-trained weights only.

Then, the utilization of semi-supervised KD further enhance the performance of CFA backbones. The proposed CSKD method achieves SOTA results on MSE, SRCC and PLCC metrics. Especially, the performance gain of ViT-Tiny is quite significant, which may be due to the sufficient model capacity but insufficient representation training

of the non-CFA backbones. The experimental results serve as implicit evidence supporting hypothesis in Section 3.2.

5.2. AADB Evaluation

In this section, the proposed two-phase approach is compared with several methods on the AADB dataset, the results are listed in Table 2. With CFA and SKD, even MV2 can significantly outperform previous SOTA TAVAR [16] that utilizing a theme branch to enhance the IAA ability. The reason for this might be attributed to the semantic information introduced through CLIP distillation.

5.3. PARA Evaluation

Table 3 shows the main results on a recently published IAA benchmark, PARA. Our approach exhibits approximately 0.1 to 0.4 improvements in terms of SRCC/PLCC compared with the previous SOTA method TAVAR [16]. With CSKD, the obtained lightweight MV2 can achieve similar results with the strategy of combining three larger models in the TAVAR method.

5.4. Interval Error Rate

The distributions of most IAA datasets are Gaussian-like imbalanced or long-tailed, leading to local unreliability of global indicators such as SRCC. In responding to this, we propose an interval-based evaluation metric to precisely identify the local performance improvement. Specifically, we split the test set into different score intervals and calculate the interval error rate (*IER*) independently,

$$IER_k = \frac{1}{N_k} \sum_{i=1}^{N_k} \mathbb{I}(|s_i^{pred} - s_i^{true}| > t), k = 0, 1, \dots, K-1. \quad (6)$$

where k and K are the index of a certain interval and the total number of intervals, respectively. N_k is the total number of samples in interval k . s_i^{pred} and s_i^{true} are the predicted and real scores of sample i . And t is a fixed threshold and is set to 0.5 in this work, referring to the error tolerance. The result is illustrated in Fig. 2.

Compared with supervised baseline, using CFA backbone can effectively reduce the error rate in the intermediate score region. The reason lies in the fact that most of the samples in IAA datasets are located in the intermediate score range, and the feature collapse problem of the CFA backbones has been alleviated, thus making the samples in this score range more discriminative. Then, SKD can further enhance the performance of well-trained CFA backbones via a large volume of unlabeled data.

6. Ablation Study

In this part, ablations are conducted to show the contribution of three key factors: 1) multi-source unlabeled dataset,

Table 1. Results on the AVA dataset. Note that NIMA* represents our replicated supervised version using ImageNet (MV2, ViT-Tiny) and ImageNet-21k (Swin-Base) pre-trained backbones, and "full" means full resolution image, up to 800 × 800 pixels. Results in blue font color indicate the SOTA performance under this metric.

| Learning scheme | Methods | Year | # Backbone | # Input size | MSE ↓ | SRCC ↑ | PLCC ↑ |
|-----------------|----------------------------|---------------------------|---|-------------------------|--------------|--------------|--------------|
| Supervised | MNA-CNN [17] | 2016 | VGG + Places205-GoogLeNet | 224 | / | / | / |
| | Kong et al. [14] | 2016 | AlexNet | 227 | / | 0.558 | / |
| | AMP [18] | 2017 | ResNet101 | full | 0.279 | 0.709 | / |
| | NIMA [27] | 2018 | VGG16 | 224 | / | 0.592 | 0.610 |
| | NIMA [27] | 2018 | Inception-v2 | 224 | / | 0.612 | 0.636 |
| | MPADA [25] | 2018 | ResNet18 | 224 [≥ 32 crops] | / | / | / |
| | Zeng et al [38] | 2019 | Supervised101 | 384 | 0.275 | 0.719 | 0.720 |
| | Hosu et al. [10] | 2019 | Inception-v3 | (full*0.875) [20 crops] | / | 0.756 | 0.757 |
| | AFDC + SPP [3] | 2020 | ResNet50 | 332 | 0.273 | 0.648 | / |
| | AFDC + SPP [3] | 2020 | ResNet50 | (224, 256, 288, 320) | 0.271 | 0.649 | 0.671 |
| | MUSIQ-single [12] | 2021 | MUSIQ | full | 0.247 | 0.719 | 0.731 |
| | MUSIQ [12] | 2021 | MUSIQ | (full, 384, 224) | 0.242 | 0.726 | 0.738 |
| | TANet [8] | 2022 | ResNet18 + MV2 | 224 | / | 0.758 | 0.765 |
| | Celona et al. [2] | 2022 | EfficientNet-B4 | 224 | / | 0.732 | 0.733 |
| | Hou et al. [11] | 2022 | [2* ResNeXt101 + ResNetv2] → ResNeXt101 | 300 | / | 0.770 | 0.770 |
| TAVAR [16] | 2023 | 2 * ResNet-50 + Swin-Base | 224 | / | 0.725 | 0.736 | |
| Supervised | NIMA* | 2018 | MV2 | 224 | 0.314 | 0.661 | 0.669 |
| | | | ViT-Tiny | 224 | 0.303 | 0.659 | 0.669 |
| | | | Swin-Base | 224 | 0.241 | 0.754 | 0.762 |
| Supervised | CFA (ours) | - | MV2 | 224 | 0.293 | 0.679 | 0.688 |
| | | | ViT-Tiny | 224 | 0.277 | 0.690 | 0.701 |
| | | | Swin-Base | 224 | 0.226 | 0.767 | 0.776 |
| Semi-Supervised | CSKD (ours) (CFA + SKD) | - | Swin-Base → MV2 | 224 | 0.272 | 0.706 | 0.717 |
| | | | Swin-Base → ViT-Tiny | 224 | 0.255 | 0.723 | 0.734 |
| | | | Swin-Base → Swin-Base | 224 | 0.224 | 0.770 | 0.779 |

Table 2. Results on the AADB Dataset.

| Methods | #Backbone | SRCC | PLCC |
|-------------------|---------------------------|--------------|--------------|
| Celona et al. [2] | EfficientNet-B4 | 0.757 | 0.762 |
| Zeng et al [38] | ResNet-50 | 0.726 | / |
| TAVAR [16] | 2 * ResNet-50 + MV3 | 0.733 | / |
| | 2 * ResNet-50 + Swin-Base | 0.763 | / |
| NIMA* | MV2 | 0.728 | 0.736 |
| | ViT-Tiny | 0.703 | 0.712 |
| | Swin-Base | 0.768 | 0.774 |
| CSKD (ours) | Swin-Base → MV2 | 0.770 | 0.780 |
| | Swin-Base → ViT-Tiny | 0.779 | 0.786 |
| | Swin-Base → Swin-Base | 0.794 | 0.798 |

2) CLIP-based feature alignment and 3) semi-supervised knowledge distillation.

6.1. Attention Analysis

Here, we follow the method in [32] to examining the layer-wise attention maps before and after CFA using ViT-Tiny backbone, results can be found in Fig. 3. The decrease in the mean attention distance of the CFA backbone, coupled with an increase in its variance, indicates a diverse and evenly representation map. Similarly, the decreased entropy suggests a greater concentration of the model. And hence,

Table 3. Results on the PARA Dataset.

| Methods | #Backbone | SRCC | PLCC |
|-------------|------------------------------|--------------|--------------|
| TAVAR [16] | 2 * ResNet-50 + Mobilenet-v3 | 0.861 | 0.902 |
| | 2 * ResNet-50 + Swin-Base | 0.911 | 0.940 |
| NIMA* | MV2 | 0.878 | 0.917 |
| | ViT-Tiny | 0.871 | 0.912 |
| | Swin-Base | 0.918 | 0.945 |
| CSKD (ours) | Swin-Base → MV2 | 0.908 | 0.937 |
| | Swin-Base → ViT-Tiny | 0.913 | 0.942 |
| | Swin-Base → Swin-Base | 0.926 | 0.951 |

these could be the reasons why the model performs better on downstream tasks.

6.2. Influences of CFA and Data Sources

In order to elucidate the benefits of introducing CFA and the impact of CLIP image encoders on CFA, we first employ CLIP ViT-B-16 and CLIP ViT-L-14 as teacher models for feature distillation. Subsequently, we exhaustively explored various combinations of ImageNet and OpenImages to validate the influence of the data source. Notably, all experiments are conducted in a supervised manner with AVA dataset, and non-CFA setting (ImageNet pre-trained weights for initialization only) is selected as the baseline.

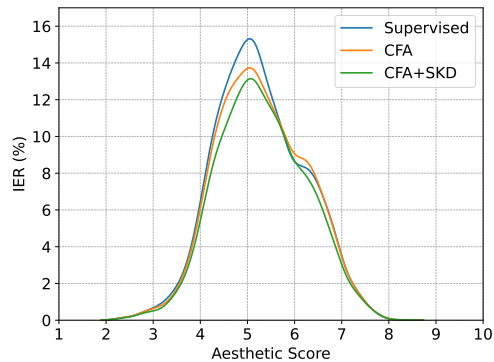


Figure 2. Interval error rate visualization on AVA dataset.

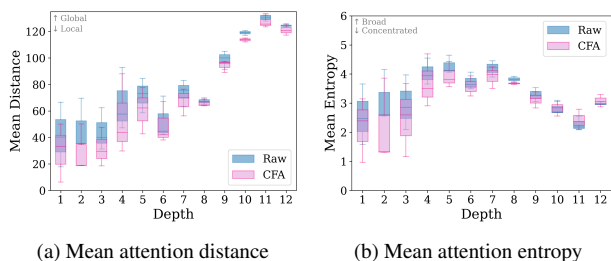


Figure 3. Mean attention distance and entropy before (raw) and after CFA, in which ViT-Tiny is selected as the backbone.

Table 4. Ablations on CFA and unlabeled data sources under supervised learning setting, AVA benchmark.

| CLIP | Dataset for CFA | Swin-Base | | MV2 | |
|----------|-----------------------|--------------|--------------|--------------|--------------|
| | | SRCC | PLCC | SRCC | PLCC |
| ✗ | ✗ | 0.754 | 0.762 | 0.661 | 0.669 |
| ViT-B-16 | ImageNet | 0.762 | 0.769 | 0.674 | 0.683 |
| | OpenImages | 0.760 | 0.768 | 0.671 | 0.681 |
| | ImageNet + OpenImages | 0.764 | 0.772 | 0.677 | 0.686 |
| ViT-L-14 | ImageNet | / | / | / | / |
| | OpenImages | / | / | / | / |
| | ImageNet + OpenImages | 0.767 | 0.776 | 0.679 | 0.688 |

In terms of CFA, experiments w/o CLIP and w/ CLIP ViT-B-16 using ImageNet for unsupervised pre-training shows the difference, the improvement on SRCC/PLCC proves the efficiency of CFA. Besides, we can see that increased CLIP size results in better performance enhancement according to experiments w/ CLIP ViT-B-16 and w/ CLIP ViT-L-14 on mixed dataset. As for the sources, experiments w/ CLIP ViT-B-16 shows that using a mixed-source dataset brings better performance.

6.3. Influence of CFA Backbones

As mentioned in Section 3.1, CFA teacher and student are obtained by unsupervised fine-tuning on ImageNet pre-trained weights, aided by a multi-source dataset. To ablate

Table 5. Results with different CFA backbones under semi-supervised learning setting (teacher: Swin-Base, student: MV2), AVA benchmark.

| | Teacher(CFA) | Student(CFA) | SRCC | PLCC |
|-----------------|--------------|--------------|--------------|--------------|
| Semi-Supervised | ✗ | ✗ | 0.698 | 0.709 |
| | ✓ | ✗ | 0.699 | 0.711 |
| | ✗ | ✓ | 0.704 | 0.714 |
| | ✓ | ✓ | 0.706 | 0.717 |

Table 6. Results of KD and SKD (Swin-Base \rightarrow MV2), AVA benchmark.

| | Labeled | Unlabeled | SRCC | PLCC |
|-----|---------|-----------------------|--------------|--------------|
| KD | AVA | ✗ | 0.690 | 0.699 |
| SKD | AVA | ImageNet | 0.701 | 0.713 |
| | AVA | OpenImages | 0.703 | 0.714 |
| | AVA | ImageNet + OpenImages | 0.706 | 0.717 |

the influence of CFA backbones under SKD setting, we conduct experiments in Table 5. Notably, symbol ✗ indicates that the backbone is initialized with ImageNet pre-trained weights without CFA, and ✓ denotes the backbone is trained in a CFA manner: first initialized with ImageNet pre-trained weights and then distilled from CLIP. In the case of using only CFA teacher or CFA student, we can observe minor improvements. The collaboration of CFA teacher and student further enhances the performance, which demonstrates the efficacy of our approach.

6.4. Ablation on KD and SKD

Table 6 gives the ablation on the influence of SKD, where supervised KD with CFA teacher and student is set as the baseline. It is clearly that SKD does outperform supervised KD, and the concatenated dataset can bring sustained benefits. This can be reasoned from two flips: 1) CFA phase optimizes the representation ability of backbones and alleviates feature collapse problem. 2) SKD can transfer more and better knowledges to the optimized backbones.

7. Conclusion

In this work, an unified CLIP-based two-phase semi-supervised scheme, CSKD, is proposed for data-hungry image aesthetics assessment tasks. Firstly, we start with a multi-source unlabeled dataset, and successfully distill the the rich features from CLIP to enhance the representation ability of the widely-used visual backbones. Subsequently, we utilize semi-supervised knowledge distillation to improve the efficiency of knowledge transfer. Finally, we conduct multidimensional ablations on CFA and SKD. Experimental results indicate the superiority of the proposed method, which we believe is a method with great potential.

References

- [1] Tom Brown, Benjamin Mann, Nick Ryder, Melanie Subbiah, Jared D Kaplan, Prafulla Dhariwal, Arvind Neelakantan, Pranav Shyam, Girish Sastry, Amanda Askell, et al. Language models are few-shot learners. *Advances in neural information processing systems*, 33:1877–1901, 2020. **1**
- [2] Luigi Celona, Marco Leonardi, Paolo Napoletano, and Alessandro Rozza. Composition and style attributes guided image aesthetic assessment. *IEEE Transactions on Image Processing*, 31:5009–5024, 2022. **5**
- [3] Qiuyu Chen, Wei Zhang, Ning Zhou, Peng Lei, Yi Xu, Yu Zheng, and Jianping Fan. Adaptive fractional dilated convolution network for image aesthetics assessment. In *Proceedings of the IEEE/CVF Conference on Computer Vision and Pattern Recognition*, pages 14114–14123, 2020. **5**
- [4] Ting Chen, Simon Kornblith, Kevin Swersky, Mohammad Norouzi, and Geoffrey E Hinton. Big self-supervised models are strong semi-supervised learners. *Advances in neural information processing systems*, 33:22243–22255, 2020. **2, 3**
- [5] Jia Deng, Wei Dong, Richard Socher, Li-Jia Li, Kai Li, and Li Fei-Fei. Imagenet: A large-scale hierarchical image database. In *2009 IEEE conference on computer vision and pattern recognition*, pages 248–255. Ieee, 2009. **3**
- [6] Dumitru Erhan, Aaron Courville, Yoshua Bengio, and Pascal Vincent. Why does unsupervised pre-training help deep learning? In *Proceedings of the thirteenth international conference on artificial intelligence and statistics*, pages 201–208. JMLR Workshop and Conference Proceedings, 2010. **2**
- [7] Yuxin Fang, Wen Wang, Binhui Xie, Quan Sun, Ledell Wu, Xinggang Wang, Tiejun Huang, Xinlong Wang, and Yue Cao. Eva: Exploring the limits of masked visual representation learning at scale. In *Proceedings of the IEEE/CVF Conference on Computer Vision and Pattern Recognition*, pages 19358–19369, 2023. **2**
- [8] Shuai He, Yongchang Zhang, Rui Xie, Dongxiang Jiang, and Anlong Ming. Rethinking image aesthetics assessment: Models, datasets and benchmarks. In *Proceeding of the Thirty-First International Joint Conference on Artificial Intelligence*, 2022. **1, 5**
- [9] Geoffrey Hinton, Oriol Vinyals, Jeff Dean, et al. Distilling the knowledge in a neural network. *arXiv preprint arXiv:1503.02531*, 2(7), 2015. **2**
- [10] Vlad Hosu, Bastian Goldlücke, and Dietmar Saupe. Effective aesthetics prediction with multi-level spatially pooled features. In *Proceedings of the IEEE/CVF Conference on Computer Vision and Pattern Recognition*, pages 9375–9383, 2019. **5**
- [11] Jingwen Hou, Henghui Ding, Weisi Lin, Weide Liu, and Yuming Fang. Distilling knowledge from object classification to aesthetics assessment. *IEEE Transactions on Circuits and Systems for Video Technology*, 32(11):7386–7402, 2022. **1, 4, 5**
- [12] Junjie Ke, Qifei Wang, Yilin Wang, Peyman Milanfar, and Feng Yang. Musiq: Multi-scale image quality transformer. In *Proceedings of the IEEE/CVF International Conference on Computer Vision*, pages 5148–5157, 2021. **1, 5**
- [13] Yan Ke, Xiaoou Tang, and Feng Jing. The design of high-level features for photo quality assessment. In *Proceedings of the IEEE Conference on Computer Vision and Pattern Recognition*, pages 419–426, 2006. **1**
- [14] Shu Kong, Xiaohui Shen, Zhe Lin, Radomir Mech, and Charles Fowlkes. Photo aesthetics ranking network with attributes and content adaptation. In *European conference on computer vision*, pages 662–679. Springer, 2016. **3, 5**
- [15] Alina Kuznetsova, Hassan Rom, Neil Alldrin, Jasper Uijlings, Ivan Krasin, Jordi Pont-Tuset, Shahab Kamali, Stefan Popov, Matteo Mallocci, Alexander Kolesnikov, et al. The open images dataset v4: Unified image classification, object detection, and visual relationship detection at scale. *International Journal of Computer Vision*, 128(7):1956–1981, 2020. **3**
- [16] Leida Li, Yipo Huang, Jinjian Wu, Yuzhe Yang, Yaqian Li, Yandong Guo, and Guangming Shi. Theme-aware visual attribute reasoning for image aesthetics assessment. *IEEE Transactions on Circuits and Systems for Video Technology*, 2023. **4, 5**
- [17] Long Mai, Hailin Jin, and Feng Liu. Composition-preserving deep photo aesthetics assessment. In *Proceedings of the IEEE conference on computer vision and pattern recognition*, pages 497–506, 2016. **5**
- [18] Naila Murray and Albert Gordo. A deep architecture for unified aesthetic prediction. *arXiv preprint arXiv:1708.04890*, 2017. **5**
- [19] Naila Murray, Luca Marchesotti, and Florent Perronnin. Ava: A large-scale database for aesthetic visual analysis. In *2012 IEEE conference on computer vision and pattern recognition*, pages 2408–2415. IEEE, 2012. **3**
- [20] Alec Radford, Jong Wook Kim, Chris Hallacy, Aditya Ramesh, Gabriel Goh, Sandhini Agarwal, Girish Sastry, Amanda Askell, Pamela Mishkin, Jack Clark, et al. Learning transferable visual models from natural language supervision. In *International conference on machine learning*, pages 8748–8763. PMLR, 2021. **1, 2**
- [21] Alec Radford, Karthik Narasimhan, Tim Salimans, Ilya Sutskever, et al. Improving language understanding by generative pre-training. *openai*, 2018. **1**
- [22] Alec Radford, Jeffrey Wu, Rewon Child, David Luan, Dario Amodei, Ilya Sutskever, et al. Language models are unsupervised multitask learners. *OpenAI blog*, 1(8):9, 2019. **1**
- [23] Robin Rombach, Andreas Blattmann, Dominik Lorenz, Patrick Esser, and Björn Ommer. High-resolution image synthesis with latent diffusion models. In *Proceedings of the IEEE/CVF Conference on Computer Vision and Pattern Recognition*, pages 10684–10695, 2022. **2**
- [24] Dongyu She, Yu-Kun Lai, Gaoxiong Yi, and Kun Xu. Hierarchical layout-aware graph convolutional network for unified aesthetics assessment. In *Proceedings of the IEEE/CVF Conference on Computer Vision and Pattern Recognition*, pages 8475–8484, 2021. **1**
- [25] Kekai Sheng, Weiming Dong, Chongyang Ma, Xing Mei, Feiyue Huang, and Bao-Gang Hu. Attention-based multi-patch aggregation for image aesthetic assessment. In *Proceedings of the 26th ACM international conference on Multimedia*, pages 879–886, 2018. **5**
- [26] Hossein Talebi and Peyman Milanfar. Learned perceptual image enhancement. In *2018 IEEE international conference*

- on computational photography (ICCP), pages 1–13. IEEE, 2018. 1
- [27] Hossein Talebi and Peyman Milanfar. Nima: Neural image assessment. *IEEE Transactions on Image Processing*, 27(8):3998–4011, 2018. 1, 3, 5
- [28] Giuseppe Valenzise, Chen Kang, and Frédéric Dufaux. Advances and challenges in computational image aesthetics. In *Human Perception of Visual Information*, pages 133–181. Springer, 2022. 1
- [29] Jianyi Wang, Kelvin CK Chan, and Chen Change Loy. Exploring clip for assessing the look and feel of images. *arXiv preprint arXiv:2207.12396*, 2022. 2
- [30] Lin Wang and Kuk-Jin Yoon. Knowledge distillation and student-teacher learning for visual intelligence: A review and new outlooks. *IEEE Transactions on Pattern Analysis and Machine Intelligence*, 2021. 2
- [31] Lin Wang and Kuk-Jin Yoon. Knowledge distillation and student-teacher learning for visual intelligence: A review and new outlooks. *IEEE Transactions on Pattern Analysis and Machine Intelligence*, 44(6):3048–3068, 2022. 2
- [32] Shaoru Wang, Jin Gao, Zeming Li, Jian Sun, and Weiming Hu. A closer look at self-supervised lightweight vision transformers. *arXiv preprint arXiv:2205.14443*, 2022. 5
- [33] Yixuan Wei, Han Hu, Zhenda Xie, Zheng Zhang, Yue Cao, Jianmin Bao, Dong Chen, and Baining Guo. Contrastive learning rivals masked image modeling in fine-tuning via feature distillation. *arXiv preprint arXiv:2205.14141*, 2022. 2
- [34] Ross Wightman. Pytorch image models. <https://github.com/rwightman/pytorch-image-models>, 2019. 3, 4
- [35] Jiachen Yang, Yanshuang Zhou, Yang Zhao, Wen Lu, and Xinbo Gao. Metamp: Metalearning-based multipatch image aesthetics assessment. *IEEE Transactions on Cybernetics*, pages 1–13, 2022. 1
- [36] Yuzhe Yang, Liwu Xu, Leida Li, Nan Qie, Yaqian Li, Peng Zhang, and Yandong Guo. Personalized image aesthetics assessment with rich attributes. In *Proceedings of the IEEE/CVF Conference on Computer Vision and Pattern Recognition (CVPR)*, pages 19861–19869, June 2022. 1
- [37] Yuzhe Yang, Liwu Xu, Leida Li, Nan Qie, Yaqian Li, Peng Zhang, and Yandong Guo. Personalized image aesthetics assessment with rich attributes. In *Proceedings of the IEEE/CVF Conference on Computer Vision and Pattern Recognition*, pages 19861–19869, 2022. 3
- [38] Hui Zeng, Zisheng Cao, Lei Zhang, and Alan C Bovik. A unified probabilistic formulation of image aesthetic assessment. *IEEE Transactions on Image Processing*, 29:1548–1561, 2019. 5
- [39] Chong Zhou, Chen Change Loy, and Bo Dai. Extract free dense labels from clip. In *Computer Vision–ECCV 2022: 17th European Conference, Tel Aviv, Israel, October 23–27, 2022, Proceedings, Part XXVIII*, pages 696–712. Springer, 2022. 2